Exciton impact-ionization dynamics modulated by surface acoustic waves in GaN

J. Pedrós*
Instituto de Sistemas Optoelectrónicos y Microtecnología and Departamento de Ingeniería Electrónica, ETSI Telecomunicación, Universidad Politécnica de Madrid, Ciudad Universitaria, 28040 Madrid, Spain

Y. Takagaki, T. Ive, M. Ramsteiner, O. Brandt, U. Jahn, and K. H. Ploog
Paul-Drude-Institut für Festkörperelektronik, Hausvogteiplatz 5-7, 10117 Berlin, Germany

F. Calle
Instituto de Sistemas Optoelectrónicos y Microtecnología and Departamento de Ingeniería Electrónica, ETSI Telecomunicación, Universidad Politécnica de Madrid, Ciudad Universitaria, 28040 Madrid, Spain
(Received 27 July 2006; revised manuscript received 15 November 2006; published 8 March 2007)

The quenching of the photoluminescence induced by the fundamental and guided high-order Rayleigh-type modes propagating in the GaN/6H-SiC(0001) heterostructure is compared. Two material types have been considered: conventional GaN and GaN underneath the Ga droplets formed during the molecular-beam-epitaxy growth. The different piezoelectric field-depth profile of each surface acoustic wave (SAW) is used to analyze their characteristics. A coupled-rate-equations model based on the impact ionization of the free and donor-bound excitons under the SAW-generated piezoelectric fields is presented, which satisfactorily reproduces the experimental results. The exciton impact-ionization rate reveals two regimes when the SAW power is increased, each of which seems to be plausibly dominated by the hole- and electron-initiated impact ionization. The SAW-induced impact-ionization model is also indicated to be valid for other wide direct band-gap piezoelectric semiconductors, such as CdS, ZnO, and AlN, where the field ionization requires an even larger electric field than in GaN.

DOI: 10.1103/PhysRevB.75.115305 PACS number(s): 78.20.Hp, 77.65.Dq, 71.35.Cc, 78.55.Cr

I. INTRODUCTION

The quenching of the near-band-gap low-temperature photoluminescence (PL) induced by surface acoustic waves (SAW) has been observed in GaAs-based systems[1–3] and GaN.[4] The piezoelectric fields accompanying the SAW ionize the photogenerated excitons confining the electrons and holes away from each other in the moving potential wells of the SAW. The spatial separation reduces the recombination probability leading to an effective PL quenching of the excitonic transitions. Field[1,2] and impact[3,4] ionization mechanisms have been proposed depending on whether the magnitude of the SAW piezoelectric fields exceeds that required for direct field ionization of an exciton in the particular material system. Although the dependence of the PL intensity of the free-exciton and impurity-bound-exciton transitions on the SAW strength has been revealed to vary differently,[1,5] their dissociation and regeneration channels are expected to be interrelated, as observed under low homogeneous dc electric fields.[6,7] Therefore, a model of the SAW-induced ionization of the distinct excitonic transitions as a coupled system is required.

Group-III nitrides are used in numerous optoelectronic systems in the visible and ultraviolet spectral ranges, such as laser and light-emitting diodes and photodetectors.[8] Moreover, nitride heterostructures stand out for the applications of SAW devices due to their large sound velocities, strong electromechanical coupling coefficients, and small temperature coefficients. Thus, the manipulation of the nitride properties by SAWs provides an efficient acousto-optoelectronic interplay.[9,10] On the other hand, SAWs are powerful probes to examine the near-surface properties of the material that supports the SAW propagation. The growth of GaN layers by molecular-beam epitaxy (MBE) is commonly carried out under Ga-rich conditions,[11] giving rise to smooth epilayer surfaces. However, Ga droplets are often formed on the surface in this growth regime, which alter the optoelectronic properties and the surface morphology of the GaN layers grown covered by them.[12] These GaN layers often present a much stronger PL than that of the GaN layers outside the droplets. In addition, the nitridation of Ga droplets themselves allows the fabrication of self-assembled GaN quantum dots.[13,14] Therefore, the evaluation of the properties of the GaN layers underneath the droplets, and their comparison with those of conventional GaN, is of great interest.

In this work, we investigate the SAW-induced PL quenching in the excitonic range of a GaN film grown by MBE on 6H-SiC(0001). We compare the quenching characteristics between the homogeneous material outside the Ga droplets and the material underneath them using spatially resolved PL. Taking advantage of the soft-film-on-hard-substrate structure of GaN/SiC, we utilize the guided modes in addition to the fundamental mode to examine the depth dependence of the exciton recombination dynamics. The experimental results are analyzed using a coupled-rate-equations model based on the impact ionization of the free and donor-bound excitons.

II. EXPERIMENT

The GaN layer used in this work was directly grown on a semi-insulating Si-face 6H-SiC(0001) substrate by plasma-assisted MBE. A rf plasma source from SVT Associates Inc. (Eden Prairie, Minnesota, USA) was used with the plasma power of 300 W and the N_2 flow rate of 0.5 sccm (sccm denotes cubic centimeter per minute at STP). Ga-rich condi-

tions were employed for the growth of a 0.97-μm-thick nominally undoped GaN layer. The sample presented a smooth and homogeneous surface except sparse areas covered by Ga droplets having a diameter of 20–30 μm. The formation of the droplets plausibly originated in a local variation of the growth temperature due to the desorption of the In used to fix the substrate to the holder. The Ga droplets were removed from the surface by a hydrochloric acid etching after the growth. Their footprints are, however, left on the surface that can be identified, for instance, by scanning electron microscopy (SEM). Throughout this paper, we denote the GaN layer inside and outside the footprints as droplet-modified- (DM-) and ordinary- (O-) GaN, respectively. The distribution of the two types of GaN is schematically illustrated in the inset of Fig. 1(b).

Single-finger interdigital transducers (IDTs) were fabricated by means of electron-beam lithography and the lift-off techniques. The IDTs had a finger width and a pitch of both 475 nm. The SAW wavelength is thus λ_{SAW}=1.9 μm. The metal electrodes were made of a 30-nm-thick Al layer with a 6-nm-thick Ti adhesion layer. Due to the hexagonal symmetry of both the wurtzite GaN film and the 6H polytype SiC(0001) substrate, the acoustic propagation in the *c*-plane is isotropic.[15] The larger sound velocity in SiC than in GaN gives rise to a confinement of acoustic modes in the epilayer. Thus, in addition to the fundamental Rayleigh-type mode, the GaN/SiC heterostructure supports guided high-order Rayleigh-type modes.[16] The calculated dispersion curves of acoustic modes for the GaN/6H-SiC structure, shown in the inset of Fig. 1(a), exhibit a good agreement with the experimentally observed resonance frequency of the fundamental, R_1, and second-order, R_2, Rayleigh-type modes (f=2.21 GHz and f=3.54 GHz at room temperature, respectively). The depth profiles of the sagittal polarization of the R_1 and R_2 modes are displayed in Figs. 1(a) and 1(b), respectively. The SAWs penetrate a few wavelengths from the surface as indicated by the particle displacement u_3 in the depth direction. The different depth profiles of the piezoelectric potential ϕ of the R_1 and R_2 modes are utilized below to examine the material properties in the droplet region at different depths.

For PL measurements, the samples were mounted in a liquid-helium cryostat equipped with rf feedthroughs. The samples were cooled down to about 10 K. Optical excitation was performed using the 325 nm line of a He-Cd laser focused to a spot having a diameter of several micrometers using a microscope objective. If the photoexcitation is too intense, the photogenerated carriers screen the SAW-induced piezoelectric fields. The measurements were thus carried out at low enough photoexcitations so that the screening was not too serious. Since the PL intensities of the DM- and the O-GaN were several orders of magnitude different, as we will see in the next section, the PL spectra from the DM-GaN region were acquired using an excitation one order of magnitude smaller than that from the O-GaN region. The PL light was collected by the same objective and analyzed using a spectrograph equipped with a cooled charge-coupled-device detector.

In order to determine the spread of the droplet modification of the GaN layer in the depth direction spatially resolved

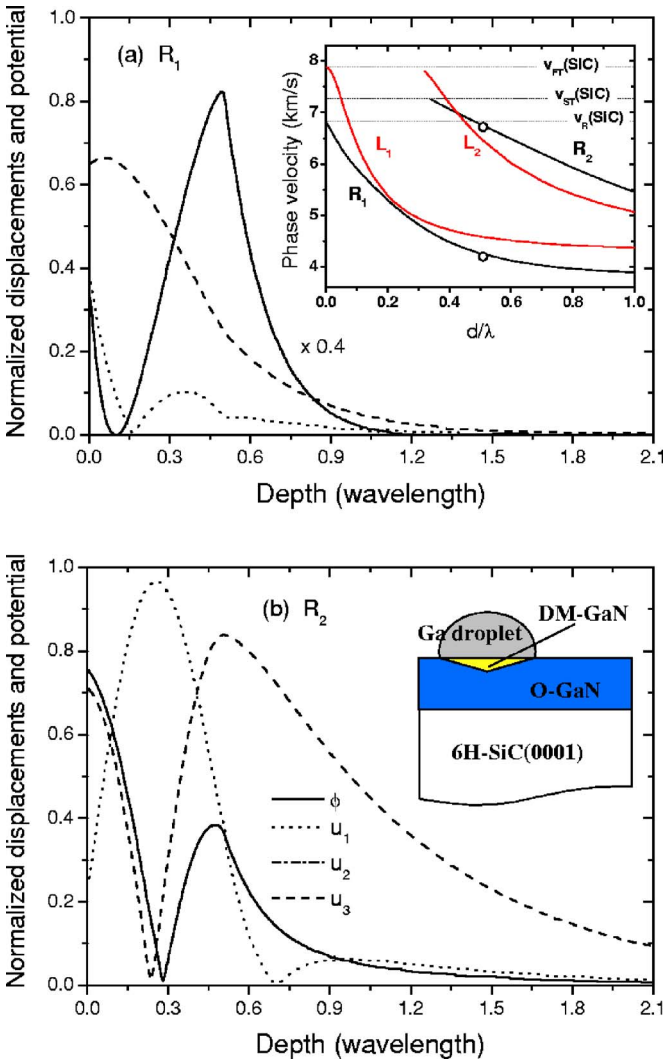

FIG. 1. (Color online) Normalized particle displacements u_i and potential ϕ of the first- (R_1), (a) and second-order (R_2), (b) Rayleigh modes in the GaN/6H-SiC heterostructure for a normalized inverse SAW wavelength d/λ=0.5. The displacements u_1, u_2, and u_3 are the longitudinal, shear horizontal, and shear vertical components, respectively. The potential in (a) has been multiplied by a factor 0.4. The inset of (a) shows the dependence of the SAW velocity on d/λ in the GaN/6H-SiC heterostructure. The solid lines show theoretical results for the two lowest-order Rayleigh (R_i) and Love (L_i) modes, whereas the symbols correspond to the experimental data. The inset of (b) is a scheme of the distribution the ordinary- (O-) and droplet-modified- (DM-) GaN layers in the GaN sample. The Ga droplets are removed by HCl etching.

cathodoluminescence (CL) measurements were carried out at a temperature of 6 K. The electron-beam energy was varied up to 13 keV with a current of about 1 nA. A grating monochromator and a cooled photomultiplier in conjunction with a conventional photon-counting technique were used to disperse and detect the CL, respectively.

III. PL SPECTRA UNDER SAW PROPAGATION

Figure 2 shows the PL spectra from the O-GaN layer. The prominent peaks at E=3.462 and 3.470 eV are associated

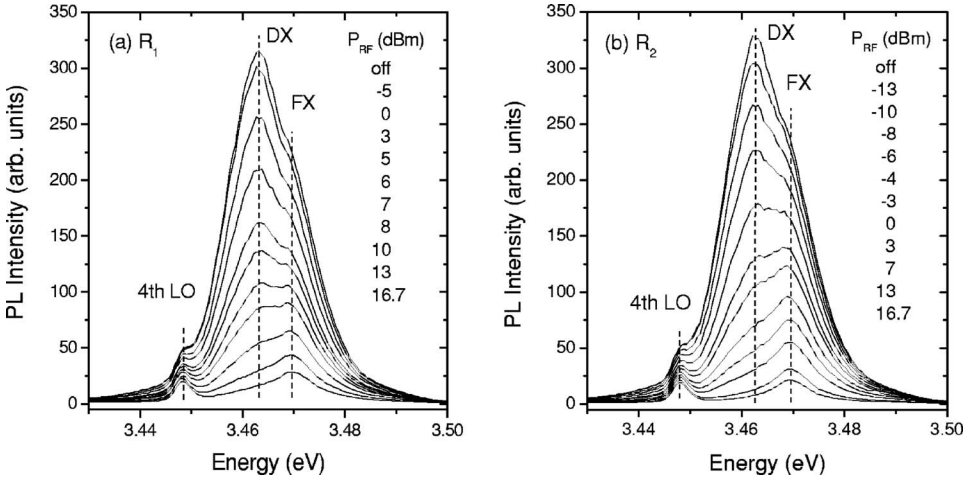

FIG. 2. Dependence of the SAW-induced PL quenching in the O-GaN layer on the rf power P_{rf} for the first- (R_1), (a) and second-order (R_2), (b) Rayleigh modes. The peaks are associated with the DX and FX transitions, and a resonant Raman transition due to the fourth-order scattering by LO phonons. The dashed vertical lines are guides for the eye.

with the donor-bound-exciton (DX) and free-exciton (FX) transitions, respectively. A resonant Raman transition due to the fourth-order scattering by longitudinal optical (LO) phonons is also observed at $E=E_{laser}-4E_{LO}=3.448$ eV, where E_{laser} is the laser excitation energy and $E_{LO}=91$ meV is the LO phonon energy.[17] In Figs. 2(a) and 2(b) the quenching of the PL when the rf power P_{rf} is increased is shown for the R_1 and R_2 modes, respectively. The "off" condition indicates that no SAW is launched and hence corresponds to the maximum PL intensity. For both of the SAW modes, the DX emission is more efficiently quenched than the FX emission. Thus, the DX peak, which dominates the PL spectra without SAW irradiation, is reduced to be below the detection limit for large values of P_{rf}, resulting in the dominance of the FX peak in the spectra. We point out that the variation of the relative strengths of the DX and FX peaks with P_{rf} differs for the R_1 and R_2 modes. We will return to this phenomenon later. The change of the PL intensity at the Raman peak due to the fourth-order LO phonon scattering is merely a consequence of the quenching of the adjacent DX peak, whose tail overlaps the Raman feature. An isolated peak at $E=3.539$ eV (not shown) due to the third-order Raman transition remains unchanged under the SAW propagation, evidencing the negligible influence of the SAW modulation on the Raman peaks.

The PL spectra from the DM-GaN layer are shown in Fig. 3. The positions of the exciton peaks are E(DX) $=3.4612$ eV and E(FX) $=3.469$ eV. The downshift in the energy compared to the peak positions for the O-GaN layer indicates a slightly higher tensile stress in the DM-GaN layer. The PL intensity for the DM-GaN layer is several orders of magnitude larger than for the O-GaN layer. No resonant Raman transitions are observed in the DM-GaN layer; plausibly they are overwhelmed by the intense excitonic features. The quenching of the PL when the P_{rf} is increased is shown in Figs. 3(a) and 3(b) for the R_1 and R_2 modes, respectively. Although the intensity of the FX peak is hardly reduced by the SAWs, the DX peak remains dominant even for the largest value of P_{rf}. The intensity ratio between the DX and FX peaks in the absence of SAWs is larger in the DM-GaN layer than in the O-GaN region. This may suggest a higher donor concentration or less compensation in the DM-GaN layer.

The stronger PL intensity of the DM-GaN layer is not related with the formation of micrometer-size single GaN crystals inside the droplets,[18] as revealed by the SEM inspection of the DM-GaN surface. Nevertheless, a lower amount of point defects induced by the nitrogen ions impinging the growth surface is expected in the DM-GaN layer as a result of the prevention of direct exposure by the Ga-droplet covering. The fewer nonradiative recombination centers give rise to a higher PL intensity. If these point defects act as acceptors, the carrier compensation will be less in the DM-GaN layer than in the O-GaN layer. In addition, an increase

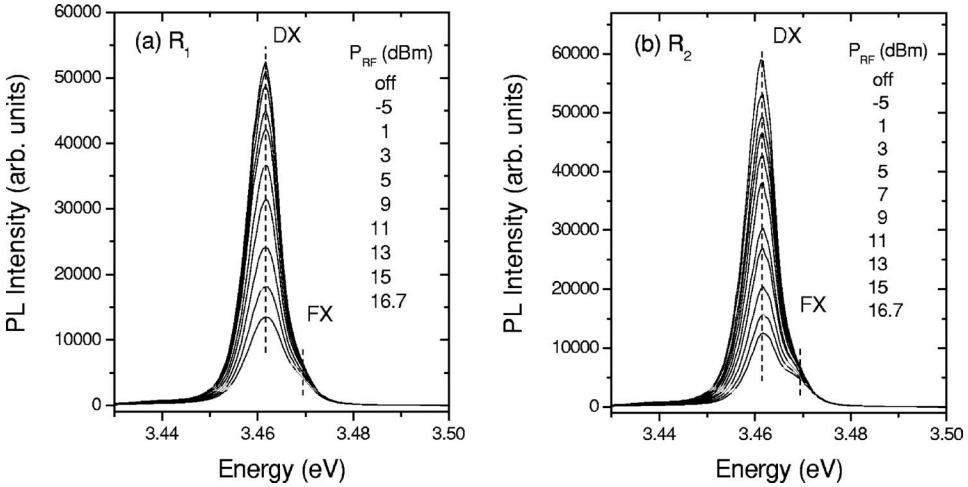

FIG. 3. Dependence of the SAW-induced PL quenching in the DM-GaN layer on the rf power P_{rf} for the first- (R_1), (a) and second-order (R_2), (b) Rayleigh modes. The peaks are associated with the DX and FX transitions. The dashed vertical lines are guides for the eye. Note that the same energy scale as in Fig. 2 has been used for comparison.

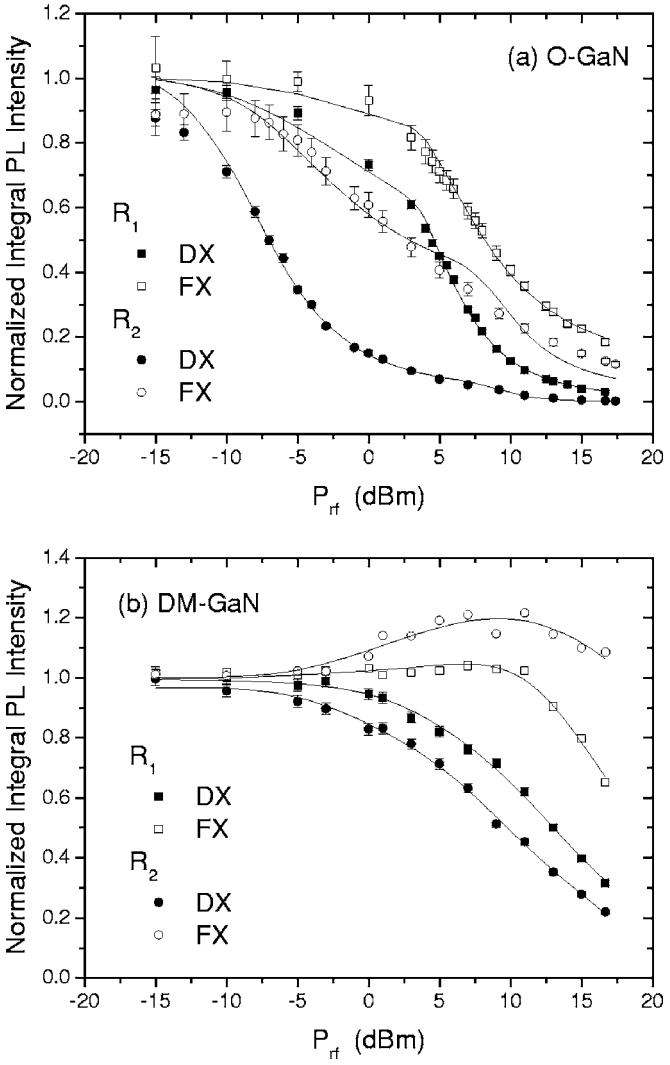

FIG. 4. Dependence of the normalized integral PL intensity of the DX and FX peaks on the rf power P_{rf} under the propagation of the first- (R_1) and second-order (R_2) Rayleigh modes, in the O-GaN, (a) and DM-GaN, (b) layers. The symbols correspond to the experimental data, whereas the lines show the best fits to the proposed model.

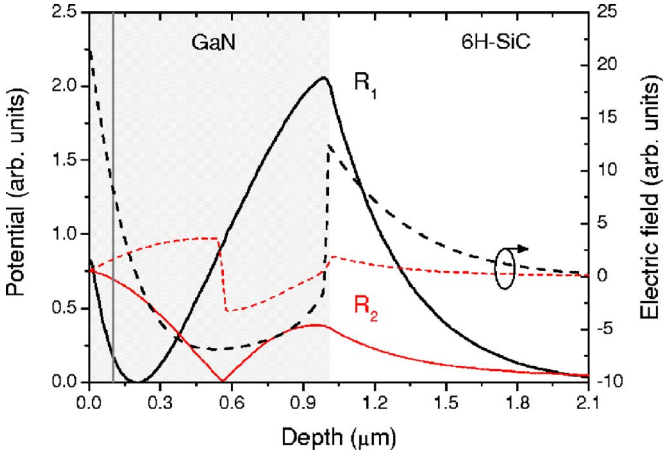

FIG. 5. (Color online) Depth profile of the potential ϕ (solid lines) and the electric field $\mathcal{E}$ (dashed lines), associated to the first- (R_1) and second-order (R_2) Rayleigh modes in the GaN/6H-SiC heterostructure for a normalized inverse SAW wavelength $d/\lambda = 0.5$. The vertical line at a depth of 100 nm indicates the optically active region, in which most of the light absorption takes place.

of the donor concentration may take place in the GaN under the droplet as oxygen will be preferentially incorporated due to its extremely N-deficient character. These mechanisms are anticipated to increase the carrier density in the DM-GaN layer. The lower efficiency in the quenching of PL by SAWs in the DM-GaN layer may originate from the carrier screening of the SAW-induced piezoelectric fields.

In order to quantitatively analyze the exciton recombinations under the SAW propagations, we have estimated the integral PL intensity of the DX and FX peaks. The intensities were calculated by fitting the PL peaks for the O-GaN layer assuming the Lorentzian profile of the exciton spectra, whereas the Gaussian profile fit better than the Lorentzian profile for the PL spectra of the DM-GaN region. The integral intensities shown in Figs. 4(a) and 4(b) for the O- and DM-GaN layers, respectively, are normalized using those in the absence of the SAW propagation.

The DX peak is quenched more efficiently than the FX peak regardless of the mode of the SAWs and the type of GaN layer. Furthermore, the FX peak is initially enhanced with increasing P_{rf} in the DM-GaN layer before the suppression eventually takes place. Such behavior was observed in PL measurements under homogeneous dc electric fields instead of the dynamic fields associated with the SAWs.[7] Irrespective of the origin of the electric fields, free carriers acquire the necessary energy to impact-ionize excitons or exciton complexes. Since the binding energy of the donor-bound exciton E_b(DX) is lower than that of the free exciton E_b(FX), the DX peak is predominantly quenched in a weak electric field. For an intense field, on the contrary, both excitons are dissociated as the free carriers are accelerated by the fields. The enhancement of the FX peak in the low-field regime is attributed to the extra free excitons generated as a consequence of the dissociation of the donor-bound excitons (DX$\rightarrow$D+FX).

One finds that there is a larger shift between the rf inputs required for the quenching of the DX and FX peaks for the R_2 mode than for the R_1 mode. The origin of this difference may lie in the contrasting depth profiles of the SAW-induced piezoelectric fields of the two modes. Figure 5 shows the calculated depth profiles of the potential ϕ (solid lines) and the electric field $\mathcal{E}$ (dashed lines) associated with the R_1 and R_2 modes. For depths smaller than 150 nm, $\mathcal{E}(R_1) > \mathcal{E}(R_2)$. From the absorption coefficient of GaN,[19] the penetration depth of the excitation laser is estimated to be around 100 nm. The free-exciton density is expected to decrease exponentially with the distance from the surface over the length scale of $\approx$100 nm. In contrast, the donor-bound-exciton density may be constant in the region close to the surface as it is restricted by the number of donors when the excitation is strong. As the SAW-induced piezoelectric field of the R_1 mode is stronger than that of the R_2 mode in the region where the free-exciton density is large, the R_1 mode would quench the FX peak more efficiently than the R_2 mode. The

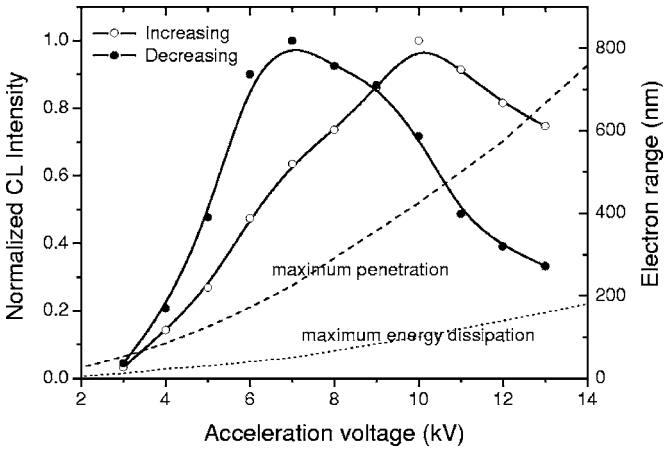

FIG. 6. Dependence of the normalized CL intensity of a footprint (DM-GaN) on the increasing (open dots) and decreasing (full dots) acceleration voltage. The solid lines are guides for the eye. For the applied dose, the electron range lies between the curves of maximum energy dissipation (dotted line) and maximum penetration (dashed line).

quenching of the donor-bound excitons would thus be less dependent on the depth profiles of the SAWs.

Figure 6 shows the CL depth profile of the DM-GaN layer obtained in a footprint. The CL intensity depends on whether the acceleration voltage is increased (open dots) or decreased (full dots). This hysteretic behavior may arise from the electron-beam-induced activation of traps. Nevertheless, both CL depth profiles reveal the localization of the DM-GaN layer within the near-surface region. The electron range has been estimated by means of Monte-Carlo simulations based on a single-electron-scattering model. The maximum energy dissipation and maximum penetration depths are plotted in Fig. 6 by dotted and dashed lines, respectively. The maximum CL intensities correspond to an averaged layer depth of 140 and 260 nm when the acceleration voltage is decreased and increased, respectively.

IV. RATE-EQUATIONS MODEL

The ionization of excitons under an electric field can be in principle produced by either field or impact ionization. The electric field needed to field-ionize a free exciton $\mathcal{E}_I(\mathrm{FX})$ must provide at least a potential drop of one effective Rydberg R across the effective Bohr radius a_B of the exciton.[20] A direct estimate of this field can be obtained assuming the effective Rydberg to be equal to $E_b(\mathrm{FX})$,[21]

$$\mathcal{E}_I(\mathrm{FX}) = \frac{R}{ea_B} \approx \frac{E_b(\mathrm{FX})}{ea_B}. \tag{1}$$

Likewise, an estimate of the electric field capable of field-ionizing a donor-bound exciton $\mathcal{E}_I(\mathrm{DX})$ is obtained considering $E_b(\mathrm{DX})$ and the radius r_{DX} of the donor-bound exciton,

$$\mathcal{E}_I(\mathrm{DX}) \approx \frac{E_b(\mathrm{DX})}{er_{\mathrm{DX}}}. \tag{2}$$

A value of 4.80 nm for the r_{DX} has been estimated using calculations of the interparticle distances of an exciton bound to a neutral donor,[22] whereas a_B=2.94 nm has been calculated for the free exciton. Binding-energy values of $E_b(\mathrm{FX})$ =26 meV and $E_b(\mathrm{DX})$=7 meV are considered.[23] According to these data, Eqs. (1) and (2) yield, respectively, an ionization field of 8.8×10^4 and 1.5×10^4 V/cm. However, in our case, the maximum values of the electric fields accompanying the SAWs in the GaN film (corresponding to the maximum power applied to the IDTs, P_{rf}=17 dBm) are below 10^4 V/cm. Thus, impact ionization is indicated to be the mechanism responsible for the exciton ionization.

We model the coupled excitonic system as shown in the inset of Fig. 7(b). The densities of free- and donor-bound excitons in the GaN layer are n_f and n_b, respectively. G and γ describe the generation and capture rates of free excitons, respectively. The excitons can be impact ionized or decay. W_f and W_b stand for the impact ionization rates of the free and donor-bound excitons, respectively. For simplicity, we do not distinguish the radiative and nonradiative decays in the emission rates, i.e., $\gamma_f=\gamma_{fr}+\gamma_{fn}$ and $\gamma_b=\gamma_{br}+\gamma_{bn}$. We do not take into account the impact ionization of neutral donors.

Under steady-state conditions, the system is described by the following rate equations:

$$\frac{dn_f}{dt} = -(\gamma + W_f + \gamma_{fr} + \gamma_{fn})n_f + W_b n_b + G = 0, \tag{3}$$

$$\frac{dn_b}{dt} = -(W_b + \gamma_{br} + \gamma_{bn})n_b + \gamma n_f = 0. \tag{4}$$

The ratio of the PL intensity of the free and donor-bound excitons is given as

$$\frac{I_f}{I_b} = \frac{\gamma_{fr}n_f}{\gamma_{br}n_b} = \frac{\gamma_{fr}}{\gamma_{br}}\frac{W_b + \gamma_{br} + \gamma_{bn}}{\gamma}. \tag{5}$$

Using the ratios in the presence and absence of the SAW transmission, W_b can be estimated as

$$\frac{\frac{I_f}{I_b} - \left.\frac{I_f}{I_b}\right|_0}{\left.\frac{I_f}{I_b}\right|_0} = \frac{W_b}{\gamma_b}. \tag{6}$$

The ionization rate W_b is expected to depend on the binding energy $E_b(\mathrm{DX})$ of the donor-bound exciton and the energy E_{SAW} carried by the SAW as

$$W_b \propto \exp\left(-\frac{cE_b(\mathrm{DX})}{E_{SAW}}\right), \tag{7}$$

where c is a constant of proportionality. We assume that $E_{SAW}\propto\mathcal{E}\propto P_{rf}^{1/2}$, where $\mathcal{E}$ denotes the electric field. One thus finds

$$\frac{\frac{I_f}{I_b} - \left.\frac{I_f}{I_b}\right|_0}{\left.\frac{I_f}{I_b}\right|_0} \propto \frac{1}{\gamma_b}\exp\left(-\frac{c'E_b(\mathrm{DX})}{P_{rf}^{1/2}}\right), \tag{8}$$

where c' is a constant of proportionality. Figures 7(a) and 7(b) show the evaluation of Eq. (8) obtained from the experi-

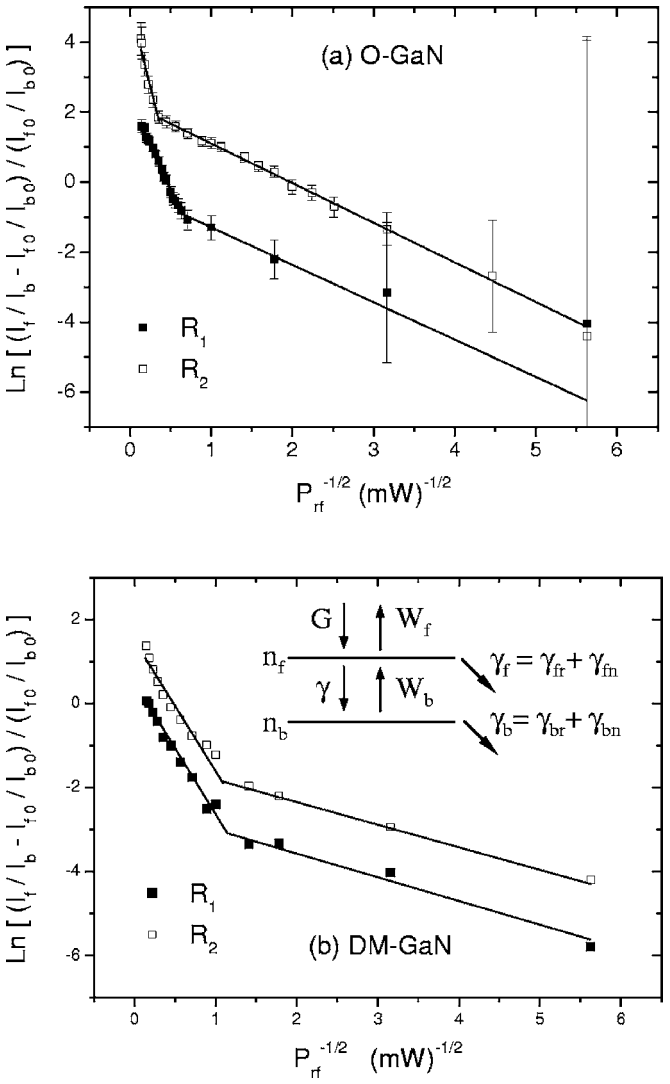

FIG. 7. Evaluation of Eq. (8) from the experimental values of the PL quenching associated with the first- (R_1) and second-order (R_2) Rayleigh modes in the O-GaN (a) and DM-GaN (b) layers. The lines show the linear fits for the low and high rf power P_{rf} regimes. The inset of (b) presents the model of the coupled excitonic system. n_f and n_b are the free-exciton and donor-bound-exciton densities, respectively. G and γ denote the generation and capture rates of free excitons, respectively. W_f and W_b stand for the impact ionization rates of the free and donor-bound excitons, respectively. The emission rates include both radiative and nonradiative decays, i.e., $\gamma_f = \gamma_{fr} + \gamma_{fn}$ and $\gamma_b = \gamma_{br} + \gamma_{bn}$.

mental values of the PL quenching induced by the R_1 and R_2 modes in the O-GaN and DM-GaN layers, respectively. For both materials and for both acoustic modes, two different linear ranges are observed, which may arise from the electron- and hole-initiated impact ionization of the excitons, since both carriers are photogenerated in the same amount. The hole-initiated impact ionization dominates at low electric fields (low P_{rf}), whereas at high electric fields the electron-initiated impact ionization gets stronger.[24] Thus, at a threshold electric field, there is a crossover resulting in a change of the slope. In the O-GaN layer [Fig. 7(a)] it occurs at a P_{rf} of 4 and 9 dBm for the R_1 and R_2 modes, respectively. The extrapolation of the two different linear regimes in the DM-GaN layer [Fig. 7(b)] yields a P_{rf} of approximately −1 and −0.5 dBm for the R_1 and R_2 modes, respectively. Thus, the crossover from one regime to the other seems to vary not only with the specific profile of the piezoelectric field accompanying each mode, but also with the transport properties of both carrier species in each material.

Both modes present similar slopes in the hole-initiated impact-ionization regime for each material, being steeper in the O-GaN layer. In the electron-initiated impact-ionization regime, both modes produce a similar increment of $\ln(W_b/\gamma_b)$ in the DM-GaN layer, whereas R_2 presents a more pronounced effect than R_1 in the O-GaN layer. According to Fig. 5, the electric field associated with the R_2 mode is lower than that of the R_1 mode in the optically active region, i.e., depth ~100 nm. However, the larger piezoelectric field associated with R_2 at larger depths may produce a large enough number of impact-ionized neutral donors to enhance the slope in this regime, as suggested by Fig. 7(a).

The normalized integral PL intensities of the donor-bound and free excitons are given by the following expressions:

$$\frac{I_b}{I_{b0}} = \frac{(\gamma+\gamma_f)\gamma_b}{(W_f+\gamma_f)(W_b+\gamma_b)+\gamma\gamma_b} = \frac{1}{A\left(\frac{W_b}{\gamma_b}\right)\left(\frac{W_f}{\gamma_b}\right)+B\left(\frac{W_b}{\gamma_b}\right)+A\left(\frac{W_f}{\gamma_b}\right)+1}, \tag{9}$$

$$\frac{I_f}{I_{f0}} = \frac{(\gamma+\gamma_f)(W_b+\gamma_b)}{(W_f+\gamma_f)(W_b+\gamma_b)+\gamma\gamma_b} = \frac{\left(\frac{W_b}{\gamma_b}\right)+1}{A\left(\frac{W_b}{\gamma_b}\right)\left(\frac{W_f}{\gamma_b}\right)+B\left(\frac{W_b}{\gamma_b}\right)+A\left(\frac{W_f}{\gamma_b}\right)+1}, \tag{10}$$

where $A=\gamma_b/(\gamma+\gamma_f)$ and $B=\gamma_f/(\gamma+\gamma_f)$. The normalized integral PL intensities of the free and donor-bound excitons under the action of the R_1 and R_2 modes, shown in Figs. 4(a) and 4(b) for the O- and DM-GaN layers, respectively, have been fitted using Eqs. (9) and (10). The impact-ionization rates W_b and W_f depend on P_{rf}, whereas the capture γ and emission rates γ_b and γ_f have been considered as constants. Equation (8) provides the functional form of W_b versus P_{rf}. A similar functional form to W_b has been assumed for W_f, but scaled in P_{rf} by a factor m related with the ratio of the binding energies of the donor-bound and free excitons, i.e., $W_f(P_{rf})=W_b(mP_{rf})$.

The lines in Figs. 4(a) and 4(b) are the resulting fitting curves for both acoustic modes in each material type. An excellent agreement with the experimental data is observed in all the cases with the exception of a slight discrepancy in the FX curve associated with the R_2 mode in the O-GaN layer at high P_{rf} values. The fitting parameters A, B, and

TABLE I. Fitting parameters A, B, and m of the normalized integral PL intensity of the DX and FX peaks under the propagation of the R_1 and R_2 modes shown in Figs. 4(a) and 4(b) for the O- and the DM-GaN layers, respectively. The FX emission (τ_f) and capture (τ) lifetimes have been calculated from the values of A and B, considering a DX emission lifetime (τ_b) of 110 ps (Ref. 25) for all the cases.

	O-GaN		DM-GaN	
	R_1	R_2	R_1	R_2
$A=\gamma_b/(\gamma+\gamma_f)$	0.82±0.03	0.27±0.04	3±1	0.4±0.2
$B=\gamma_f/(\gamma+\gamma_f)$	0.4±0.2	0.7±0.1	0.43±0.06	0.56±0.04
m	0.94±0.04	0.87±0.07	3.6±0.9	3.7±0.9
τ_b (ps)	110	110	110	110
τ_f (ps)	225	40	770	80
τ (ps)	150	100	580	100

m, obtained in each material type and acoustic mode are summarized in Table I. The free-exciton emission and capture lifetimes, τ_f and τ, respectively, have been calculated from the values of A and B considering a donor-bound exciton-emission lifetime τ_b of 110 ps (Ref. 25) for all the cases. The values of τ_f and τ arising from this calculation present similar values in both material types for the R_2 mode, whereas they considerably differ in the case of the R_1 mode (see Table I). This fact can be understood considering the distinct electric-field depth profiles associated with each mode. The electric field associated with the R_2 is very weak in the region close to the surface. Since the DM-GaN layer has a main surface character, as indicated by its CL depth profile shown in Fig. 6, the R_2 mode likely provides its major response from the GaN below the droplet region. Hence, the R_2 mode assesses the bulk GaN behavior, which is similar in both material types, as shown in the inset of Fig. 1(b). Conversely, the electric field associated with the R_1 mode is more intense in the region close to the surface, efficiently evaluating the topmost GaN layer. Thus, the largest value of τ_f, obtained in the DM-GaN layer with the R_1 mode, confirms the better crystal quality of this layer and the suitability of the R_1 mode as a surface probe.

The scaling factor m between the functional forms of W_b and W_f is expected to correspond with the ratio $E_b(\mathrm{FX})/E_b(\mathrm{DX})$. $E_b(\mathrm{DX})$ is in the range of 6–7.5 meV,[23,26,27] whereas $E_b(\mathrm{FX})$ presents some dispersion in the literature, with values in the ranges of 20–21 meV (Refs. 26 and 28) and 25–26.5 meV.[23,29] Thus, the value of $m\approx 3.6$ obtained in the DM-GaN layer is consistent with the model assumptions. However, the value of $m\approx 0.9$ obtained in the O-GaN layer indicates that, in this case, our model is too simplified. The more intense SAW-induced piezoelectric field in the O-GaN layer may impact-ionize neutral donors, which present a binding energy $E_b(\mathrm{D})$ of 30–33 meV for the most common shallow donors.[23,30] Additional dissociation paths are foreseen, namely, $\mathrm{DX}\rightarrow \mathrm{D}^+\mathrm{X}+\mathrm{e}$ and $\mathrm{DX}\rightarrow \mathrm{D}+\mathrm{e}+\mathrm{h}$.[6] Nevertheless, the first is not resolved in the PL spectra, whereas the second would require hot carriers capable of providing an energy above 36.3 meV.[23]

TABLE II. Electric field capable of field ionizing a free exciton $\mathcal{E}_I(\mathrm{FX})$ estimated from Eq. (1) for different piezoelectric semiconductors. The values of the effective Bohr radius a_B and the binding energy $E_b(\mathrm{FX})$ of the free exciton are taken from Ref. 20 for GaAs, Refs. 31 and 32 for CdS, Ref. 33 for Zn0, and Refs. 34 and 35 for AlN, whereas those of the band-gap energy E_g are approximate values at 300 K.

	E_g (eV)	a_B (nm)	$E_b(\mathrm{FX})$ (meV)	$\mathcal{E}_I(\mathrm{FX})$ (V/cm)
GaAs (cubic $\bar{4}3m$)	1.43	8.9	5.1	5.7×10^3
GaN (hexagonal $6mm$)	3.4	2.94	26	8.8×10^4
CdS (hexagonal $6mm$)	2.4	2.8	29	1.0×10^5
ZnO (hexagonal $6mm$)	3.4	1.8	60	3.3×10^5
AlN (hexagonal $6mm$)	6.2	1.9	80	4.2×10^5

The presented model of the SAW-induced impact ionization of excitons in GaN is expected to be valid for other wide direct-band-gap piezoelectric semiconductors, such as CdS, ZnO, and AlN. These materials present higher free-exciton binding energies and lower effective Bohr radii than those in GaN, thus requiring even larger electric fields to field-ionize a free exciton, as shown in Table II.

V. CONCLUSIONS

We have investigated the SAW-induced PL quenching in the excitonic range of a GaN film grown by MBE on SiC under specific Ga-rich conditions in which Ga droplets are formed. The quenching characteristics of the homogeneous material outside the Ga droplets and the material underneath them (O- and DM-GaN, respectively) have been compared. The DM-GaN layer presents an outstandingly high PL intensity, likely related to a reduction of point defects induced by the plasma-source nitrogen ions, due to the protective covering provided by the Ga droplet. The first- and second-order Rayleigh modes arising in the GaN/SiC heterostructure have been used to evaluate both material types. Their different piezoelectric-field depth profiles have allowed the scan of the GaN film at distinct depths. The SAW-based analysis has pointed out the main surface character of the DM-GaN layer, as confirmed by CL depth profiling. The exciton impact-ionization dynamics under the SAW-generated piezoelectric fields has been satisfactorily reproduced using a coupled-rate-equations model. The exciton impact-ionization rate presents two linear regimes when the SAW power is increased, each of which is plausibly dominated by the hole- and electron-initiated impact ionizations.

ACKNOWLEDGMENTS

The authors wish to thank E. Wiebicke for technical support. This work has been partially supported by the Spanish Ministerio de Educación y Ciencia (Projects No. TIC2001-2794 and No. TEC2004-05698-C02-01/MIC).

*Email address: jpedros@die.upm.es

[1] K. S. Zhuravlev, D. V. Petrov, Y. B. Bolkhovityanov, and N. S. Rudaja, Appl. Phys. Lett. **70**, 3389 (1997).
[2] C. Rocke, S. Zimmermann, A. Wixforth, J. P. Kotthaus, G. Böhm, and G. Weimann, Phys. Rev. Lett. **78**, 4099 (1997).
[3] P. V. Santos, M. Ramsteiner, and F. Jungnickel, Appl. Phys. Lett. **72**, 2099 (1998).
[4] J. Camacho, P. V. Santos, F. Alsina, M. Ramsteiner, K. H. Ploog, A. Cantarero, H. Obloh, and J. Wagner, J. Appl. Phys. **94**, 1892 (2003).
[5] C. Rocke, A. O. Govorov, A. Wixforth, G. Böhm, and G. Weimann, Phys. Rev. B **57**, R6850 (1998).
[6] W. Bludau and E. Wagner, Phys. Rev. B **13**, 5410 (1976).
[7] D. Nelson, B. Gil, M. A. Jacobson, V. D. Kagan, N. Grandjean, B. Beaumont, J. Massies, and P. Gibart, J. Phys.: Condens. Matter **13**, 7043 (2001).
[8] A. Yasan and M. Razeghi, in *Optoelectronic Devices: III-Nitrides*, edited by M. Razeghi and M. Henini (Elsevier, Oxford, 2004), Chap. 9, pp. 213–249; R. McClintock and M. Razeghi, in *ibid.*, Chap. 10, pp. 251–284.
[9] D. Ciplys, R. Rimeika, M. S. Shur, S. Rumyantsev, R. Gaska, A. Sereika, J. Yang, and M. A. Khan, Appl. Phys. Lett. **80**, 2020 (2002).
[10] T. Palacios, F. Calle, and J. Grajal, Appl. Phys. Lett. **84**, 3166 (2004).
[11] C. Adelmann, J. Brault, D. Jalabert, P. Gentile, H. Mariette, G. Mula, and B. Daudin, J. Appl. Phys. **91**, 9638 (2002).
[12] C. Kruse, S. Einfeld, T. Böttcher, D. Hommel, D. Rudloff, and J. Christen, Appl. Phys. Lett. **78**, 3827 (2001).
[13] K. Kawasaki, D. Yamazaki, A. Kinoshita, H. Hirayama, K. Tsutsui, and Y. Aoyagi, Appl. Phys. Lett. **79**, 2243 (2001).
[14] C. W. Hu, A. Bell, F. A. Ponce, D. J. Smith, and I. S. T. Tsong, Appl. Phys. Lett. **81**, 3236 (2002).
[15] J. Pedrós, F. Calle, J. Grajal, R. J. Jiménez Riobóo, Y. Takagaki, K. H. Ploog, and Z. Bougrioua, Phys. Rev. B **72**, 075306 (2005).
[16] Y. Takagaki, P. V. Santos, E. Wiebicke, O. Brandt, H. P. Schönherr, and K. H. Ploog, Phys. Rev. B **66**, 155439 (2002).
[17] A. Kaschner, A. Hoffmann, and C. Thomsen, Phys. Rev. B **64**, 165314 (2001).
[18] J. Menniger, U. Jahn, O. Brandt, H. Yang, and K. Ploog, Phys. Rev. B **53**, 1881 (1996).
[19] J. F. Muth, J. D. Brown, M. A. L. Johnson, Z. Yu, R. M. Kolbas, J. W. Cook, Jr., and J. F. Schetzina, MRS Internet J. Nitride Semicond. Res. **4S1**, G5.2 (1999).
[20] D. F. Blossey, Phys. Rev. B **2**, 3976 (1970).
[21] A. Wixforth, Physica E (Amsterdam) **3**, 145 (1998).
[22] M. Suffczynski and L. Wolniewicz, Phys. Rev. B **40**, 6250 (1989).
[23] O. Brandt, J. Ringling, K. H. Ploog, H. J. Wünsche, and F. Henneberger, Phys. Rev. B **58**, R15977 (1998).
[24] I. H. Oguzman, E. Belloti, K. F. Brennan, J. Kolník, R. Wang, and P. P. Ruden, J. Appl. Phys. **81**, 7827 (1997).
[25] G. Pozina, N. V. Edwards, J. P. Bergman, T. Paskova, B. Monemar, M. D. Bremser, and R. F. Davis, Appl. Phys. Lett. **78**, 1062 (2001).
[26] M. Smith, G. D. Chen, J. Z. Li, J. Y. Lin, H. X. Jiang, A. Salvador, W. K. Kim, O. Aktas, A. Botchkarev, and H. Morkoc, Appl. Phys. Lett. **67**, 3387 (1995).
[27] R. A. Mair, J. Li, S. K. Duan, J. Y. Lin, and H. X. Jiang, Appl. Phys. Lett. **74**, 513 (1999).
[28] W. Shan, A. J. Fischer, S. J. Hwang, B. D. Little, R. J. Hauenstein, X. C. Xie, J. J. Song, D. S. Kim, B. Goldenberg, R. Horning, S. Krishnankutty, W. G. Perry, M. D. Bremser, and R. F. Davis, J. Appl. Phys. **83**, 455 (1998).
[29] S. J. Xu, W. Liu, and M. F. Li, Appl. Phys. Lett. **81**, 2959 (2002).
[30] J. A. Freitas, Jr., W. J. Moore, B. V. Shanabrook, G. C. B. Braga, S. K. Lee, S. S. Park, and J. Y. Han, Phys. Rev. B **66**, 233311 (2002).
[31] D. G. Thomas and J. J. Hopfield, Phys. Rev. **116**, 573 (1959).
[32] Y.-M. Yu, K.-M. Kim, B. O, K.-S. Lee, Y. D. Choi, and P. Y. Yu, J. Appl. Phys. **92**, 1162 (2002).
[33] S. Hong, T. Joo, W. Park, Y. H. Jun, and G.-C. Yu, Appl. Phys. Lett. **83**, 4157 (2003).
[34] T. Onuma, S. F. Chichibu, T. Sota, K. Asai, S. Sumiya, T. Shibata, and M. Tanaka, Appl. Phys. Lett. **81**, 652 (2002).
[35] K. B. Nam, J. Y. Lim, and H. X. Jiang, Appl. Phys. Lett. **82**, 1694 (2003).